

## Computational Analysis of Towed Solar Platform Aircraft

### Abstract

The use of single-sheet planform areas on aircraft can enable both lighter weight construction by eliminating internal wing structures and increased solar power collection through use of bifacial photovoltaic sheets (“bifacial sheets”); the result is >4X Watts of collected solar energy per kilogram of structure. For single-sheet construction, structural constraints teach toward low aspect ratio designs that do not rely on lift forces being transferred crosswise across wingspans, enabled by towed platform technology. The challenge is developing good aerodynamic lift at aspect ratios of 1.0 and lower.

Simulation of digital prototypes identified that the distributed propulsion technologies of Lift Span Tech and cross-over propulsor are particularly effective in single-sheet planform designs. Towed platform technology enables flexible designs that are robust. The combination of robustness and good performance enable 24/7 flight and day missions from the same design.

When combined with distributed propulsion, bifacial sheets can displace battery weight, increase lift, prevent boundary layer separation, enable lower-aspect-ratio aircraft at high  $L/D$  efficiency, and enable takeoff and landing over shorter and more-diverse surfaces.

### Nomenclature

2D	=	two dimensional.
3D	=	three Dimensional
AoA	=	air’s angle of attack (°)
<b>AR</b>	=	aspect ratio, defined as the span divided by a representative longitudinal chord length
Camber	=	curvature of an airfoil characterized as a deviation from straight as a either a fraction of the chord length or percent of a chord length (e.g., 0.01 c or 1%)
<b>CFD</b>	=	computational fluid dynamics
c, Chord	=	chord, distance from leading edge to trailing edge of an airfoil or wing
$C_l, C_d$	=	lift and drag coefficients
Gap Ratio	=	Ratio of airfoil thickness to the distance between the lowest part of the airfoil and the ground.
$L/D$	=	lift-drag ratio, the primary measure of airframe efficiency; $L/D$ is calculated as the CFD lift coefficient divided by the drag coefficient.
lift pressures	=	pressures that generate aerodynamic lift such as lower pressures on upper surfaces and higher pressures on lower surfaces.
NACA0006	=	an airfoil shape defined by NACA standards with a t/c of 0.06
<b>P</b>	=	pressure (N/m <sup>2</sup> )
PIC	=	particle image velocimetry
<b>S</b>	=	abbreviation for “source” which is a source of air-based propulsion.
STL	=	stereolithography, file generated by computer aided design software
<b>U, u</b>	=	velocity.
t/c	=	thickness to chord ratio, thickness is a maximum vertical dimension
VTOL	=	vertical takeoff and landing
$\alpha_A$	=	angle from horizontal (°), subscript A identifies an airfoil pitch angle with nose up

as positive

## Introduction

When a single sheet replaces a wing, the sheet replaces upper and lower wing skins and internal structures resulting in a 50% to 70% reduction in areal density ( $\text{kg/m}^2$ ). Applying a bifacial photo-voltaic (PV) panel as the single sheet allows solar energy to be collected from upper and lower surfaces at a magnitude of 1.2 to 1.8 times the areal solar power ( $\text{W/m}^2$ ) of single surface photo-voltaic panels [1]. The result is 2.4X to 6X the solar power density ( $\text{W/kg}$ ) than contemporary wing-based solar panels.

The challenge is to create high lift-drag ratio ( $L/D$ ) lifting bodies from robust aircraft platforms consisting of substantive single-sheet planform areas. Known designs for laterally extending wings require internal structures for spanwise transfer of lift forces. Longitudinally-extending planforms are able to avoid issues with spanwise transfer of lift forces and use streamlined ribs to transfer forces longitudinally while preserving substantive bifacial sheet planform area. These ribs may serve additional purposes such as housing batteries or microelectronics with minimal drag penalties relative to other configurations. The ribs may balance flexibility with structural conformality to maintain robustness while providing good aerodynamic lift configurations.

Additional benefits may arise with manufacturing capabilities that enable mass-produced PV sheets to be directly used as lifting bodies that displace the costs of other materials and structures used for aircraft skins and structures. Compatible electric motors should cost and weigh less than combustion engines. A goal would be for vehicle costs to be equal to or lower than current vehicle costs while using bifacial lifting-body sheets to eliminate fuel costs as well as reduce maintenance and infrastructure costs associated with combustion engines.

This paper evaluates the use of distributed propulsion on thin cambered panels (i.e., sheets) to create effective lifting bodies of high  $L/D$  efficiency.

## Background

**Deficiencies of Thin-Cambered Airfoils** – In addition to a lack of compression strength necessary to transfer lateral loads, thin cambered sheets have greater dissipation of  $L/D$  efficiency than NACA-type wings. Wing sections rely on induced thrust at forward sections to nullify induced drag at trailing sections to create high  $L/D$  efficiencies. For thin cambered airfoils operating at ideal 2D performance, induced thrust on the lower-surface front section substantially cancels the induced drag on the lower-surface trailing section.

For lower-aspect-ratio lifting bodies, the spanwise loss of lift pressures from the lower surface leads to disproportionately greater increased induced drag versus induced thrust resulting in rapidly decreasing  $L/D$  efficiency [2-5]. NACA-type wings and filled-camber wings do not have this rapidly deteriorating  $L/D$  efficiency and have emerged as preferred lifting body configurations [6].

The camber of thin cambered lifting bodies is able to continuously generate lift along the length to compensate for the continuous loss of lift in vertical and lateral directions. However, higher camber leads to greater magnitude pitches at leading and trailing edges which exacerbates the rapid deterioration of  $L/D$  efficiency as aspect ratio decreases.

Therefore, while several works have identified that thin cambered airfoils are able to generate  $L/D$  efficiencies in excess of 40 they have determined there is minimal application; High aspect ratio lifting bodies built with thin cambered designs lack the ability to transfer load across to a wing root to suspend a fuselage [7-11]. For low aspect ratio designs, spanwise losses have especially detrimental impacts on performance due to the loss of lift pressures and transformation of surfaces near the leading edge from providing induced thrust to causing induced drag. For low aspect ratio designs, performance needs to be supplemented with approaches like distributed propulsion in application [12-19].

**A Solution with Distributed Propulsion** – Air-based propulsion, e.g. ducted fans and jet engines, generate pressures on blades where intake and discharge surfaces direct the expansion of pressures into velocities. A typical interpretation of propulsors is that the momentum resulting from air's increased velocity creates thrust.

A more detailed interpretation is that pressures created on blades enact force on the blade surface area to create thrust. At intake scoops and discharge nozzle bells, the pressures can directly or indirectly (i.e. through pressure-velocity transformation) create lower pressures and higher pressures that can create thrust in a coupled and complementary mechanism.

The details of surface configurations as coupled with propulsor power determine the overall efficiency of the engine and surrounding surfaces for creating propulsion. However, a key metric on the efficiency is the amount of lost work in the air streamlines behind the propulsor and respective aft surfaces of the bodies to which the propulsor is attached.

Waste heat is one form of lost work, but the most-relevant metrics related to propulsor-surface interactions is lower-pressure lower-longitudinal-velocity turbulence from boundary layer separation and higher-velocity jet wash. The most inefficient designs can produce both boundary-layer-separation turbulence and jet wash in aft streamlines. An active area to address boundary layer separation and turbulence issues with wings and aircraft include shape optimization and the addition of morphing surfaces [20-23].

Effective designs will exhibit an optimal power setting which creates aft streamlines of uniform pressure and velocity at free-stream pressure and velocity [24]. Absent jetwash, it is still possible to create net thrust from lower pressures forward the propulsor acting on upper surface areas of negative pitch. A technology using this approach is referred to as Lift Span Tech is based on near-horizontal surfaces in front to a propulsor and a trailing taper aft the propulsor. Lift Span Tech includes use of morphing surfaces to vary surface pitches as a function of propulsor power. Lift Span Tech can be applied to thin cambered surfaces [25].

Cross-over propulsors can also be used with thin cambered wings. An overall objective of a cross-over propulsor is to reset flow patterns for an extended long-chord thin-cambered airfoil to avoid forming steeper pitch surfaces (e.g.  $<-3^\circ$  and  $> 3^\circ$ ) except as configured with the propulsor to generate induced thrust or alleviate induced drag.

**Towed Platform Technology** – High solar power densities of single-sheet platform areas enable solar aircraft designs with increased solar power available for missions versus the power needed to sustain the flight of the PV cells. Increased excess power enables higher velocities, extended flight, higher altitudes, and more-versatile designs for 24/7 aircraft.

One problem encountered with low-aspect-ratio relatively-flat lifting bodies is pitch instability where perturbances can cause the leading edge to flip up and over the trailing edge. A platform towed from the leading edge exhibits passive stability similar to trailers pulled by trucks. A forward axial pivot connection on the towed platform creates pitch stability on the towed platform while retaining roll control forces. Figure 1 illustrates 2021 and 2024 versions of a towed platform.

Four improvements from 2021 to 2024 designs are: a) use of cambered platforms rather than flat platforms, b) use of a crossover propulsor, c) use of a trailing-edge propulsor, and d) use of laterally extending wings on the lead aircraft. The following are advantages of these improvements:

- a) The camber creates a continuous source of impacting and diverging air flows that continuously generate aerodynamic lift along the chord versus a flat plate where flow parallel to the surface develops so lift forces continue to dissipate without replenishment.
- b) A crossover propulsor generates lower pressures on upper-surface areas in front of the intake and higher-pressures on lower surfaces aft the intake.
- c) A trailing-edge propulsor generates lower pressures on upper-surface areas in front of the intake and higher pressures aft the propulsor which can benefit **L/D** efficiency.
- d) A lead aircraft with laterally extending wings can use the wings to generate lift for a payload while slowing the loss of lift pressure on the inboard sections.

Multiple towed platforms could be extended in series; where in principle, an increasing train of platforms creates additional surplus power. This technology could enable aircraft as stratospheric manufacturing platforms and sustainable launch hubs for access to space.

This paper uses computational fluid dynamics to provide insight into how distributed propulsion can be used to enhance the **L/D** efficiency of single-sheet lifting bodies.

**Power Ratio Calculations** - The Power Ratio is the ratio of power delivered ( $W_{SP} * P_{PV}$ ) divided by the power to sustain flight ( $g * W_{SP} * D/L * U$ ), both in  $W/m^2$ . Equation 1 provides this ratio in equation form.

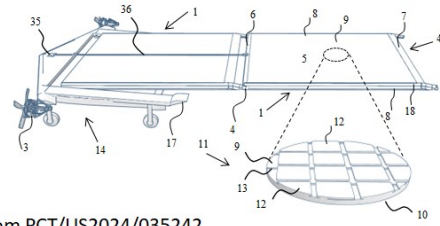
$$Power\ Ratio = \frac{P_{PV}}{g \rho_{PV} (D/L) U} \left( \frac{W/m^2}{\frac{m}{s^2} \frac{kg}{m^2} \frac{m}{s}} \right) \quad (1)$$

Where:  $g = 9.8 \text{ m/s}^2$ ,

$P_{PV}$  is power density of photovoltaic array including wing weight ( $W/m^2$ ).

$\rho_{PV}$  is specific mass of a sheet in  $kg/m^2$ .

From PCT/US2021/016392



From PCT/US2024/035242

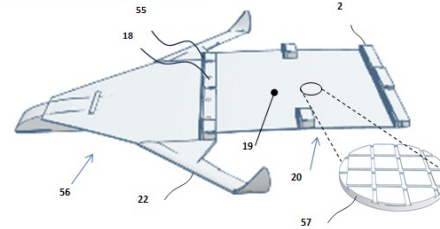


**Figure 1.** Versions of solar aircraft (a, 2021, b. 2024) using solar platforms from PCT/US2021/016392.

$U$  is velocity (m/s) with benchmarks of 343 for sound and 250 for commercial airliner.  
 $L/D$  is lift-drag ratio (i.e., 3D airfoil performance),

Tables 1 and 2 provide compiled data used to estimate the performance available from commercial products for solar power collection and wing construction with projections for PV sheets used as lifting bodies. Typical specific masses ( $\text{kg}/\text{m}^2$ ) of complete solar aircraft are about  $2 \text{ kg}/\text{m}^2$  versus thin cambered planform areas at  $0.076$  to  $0.114 \text{ kg}/\text{m}^2$  per Table 2 [26, 27].

**Table 1.** Properties of photovoltaic panels.

Property	Value	Sources of Data
Power Density, $P_{PV}$ (W/kg)	150	<a href="https://www.spectrolab.com/photovoltaics.html">https://www.spectrolab.com/photovoltaics.html</a> (honeycomb)
	1000	<a href="https://www.spectrolab.com/photovoltaics.html">https://www.spectrolab.com/photovoltaics.html</a> (thin film, expensive)
Efficiency	30%	Microlink <a href="http://mldevices.com">http://mldevices.com</a>
	22%	<a href="https://us.sunpower.com/">https://us.sunpower.com/</a>
	30%-32%	<a href="https://www.spectrolab.com/photovoltaics.html">https://www.spectrolab.com/photovoltaics.html</a>
	40%	<a href="https://www.spectrolab.com/photovoltaics.html">https://www.spectrolab.com/photovoltaics.html</a>
Surface Weight ( $\text{g}/\text{m}^2$ )	350	Microlink <a href="http://mldevices.com">http://mldevices.com</a>
Sun Radiation (W/kg)	100-230	$\text{W}/\text{m}^2$ , from cloudy locations (100) to desert locations (230). [28]
	120%	factor: solar radiation at higher altitudes.[28]
	150% (120%-180%)	factor: bifacial photovoltaic sheets including reflection; Reflective ground and clouds, not inclusive of higher altitude radiation.

**Table 2.** Towed Platform mass breakdown for  $10\text{m}^2$  [26].

Element	Contemporary Wing (kg)	Towed Platform (kg) (strong spar extension)	Towed Platform (kg) (some spar extension)
Ribs	0.22	0.18	0.05
Spars	1.09	0.55	0.30
Skin	0.82	0.41	0.41
Boom	0.15	N/A	N/A
Total	2.28 kg ( $0.228 \text{ kg}/\text{m}^2$ )	1.14 kg ( $0.114 \text{ kg}/\text{m}^2$ )	0.76 kg ( $0.076 \text{ kg}/\text{m}^2$ )

Based on these summaries, a reasonable value for Photovoltaic cell productivity above the clouds is:  $120\% * 150\% * 200 \text{ W}/\text{m}^2$ , or  $P_{PV} = 360 \text{ W}/\text{m}^2$  with higher altitude radiation, reflective clouds, and full solar exposure.

Example application scenarios include:

- A towed platform acting as a power source to a lead aircraft at  $L/D=20$  and velocity of  $40 \text{ m}/\text{s}$ ; ( $89.5 \text{ mph}$ ) the power source produces  $360 \text{ W}/\text{m}^2 \times [20 / (9.8 \text{ m}/\text{s}^2 \times 0.076 \text{ kg}/\text{m}^2 \times 40 \text{ m}/\text{s})]$ , or  $Power Ratio = 536$ .
- A towed platform acting as a power source to a lead aircraft at  $L/D=20$  and velocity of  $120 \text{ m}/\text{s}$ ; ( $268 \text{ mph}$ ) the  $Power Ratio = 179$ .

These calculations indicate that the power ratio of a PV sheet is much greater than is needed to sustain flight with excess power for storing in batteries and other functions. This indicates that battery and equipment weight is a more critical factor than the weight of the bifacial sheets.

Thin cambered planform technology is a high-impact technology with applications ranging from:

- towed panel technology to power lead aircraft trailing panels for specific applications to
- supplementing electric aircraft, such as passenger aircraft, to extend range and reduce battery weights and costs.

## Methods

OpenFOAM and Simflow CFD software were used to simulate digital prototypes from prepared STL files. Methods were matched to maintain fidelity and methods analogous to those within the field [3, 11, 29]. Two-dimensional (2D) simulations were used to identify trends in performance while 3D simulations were performed on the final prototypes and key designs. Unless otherwise reported, the scale chords of the STLs were 1 m, the fluid was air at 1 atm pressure, and the free stream velocity was 40 m/s.

In these studies, the “thin” cambered wing sections are STL models that are as thin as possible without leading to erroneous meshing results. Typically, the sheet thickness to chord is about 0.5:100.

Pressure profiles are symmetrically presented with blue as low pressures, red as high pressures, and passing through green at 0-gauge pressure. Computer aided design (CAD) was used to create STL files by combining common geometries.

Velocity profiles are from the reference frame of the airfoil/digital prototype. Free steam flow boundaries were simulated at a minimum of 10 chord lengths from the vehicle in free stream directions.

Both 2D and 3D CFD simulations were performed. 2D simulations are referred to as being performed on airfoils or wing sections. 3D simulations are referred to as being performed on digital prototypes.

## Results

**Outline of Results** – The results of this work include multiple cycles of studies toward the result of understanding how aircraft platforms with large planform areas of single-bifacial sheet construction may be used to yield both high solar power densities ( $W/kg$ ) and  $L/D$  efficiencies in excess of 20:1. The scope includes the following:

- 1) Basic studies on thin cambered wing sections including discussion.
- 2) Basic studies on distributed propulsion including discussion.
- 3) Basic studies leading to Lift Span Technology, including discussion.
- 4) Wing section studies on two thin cambered airfoils in sequence with a cross-over propulsor and trailing-edge upper-surface propulsor.
- 5) [Gain]:[loss] ratio analysis of using distributed propulsion where the gain is effective thrust realized on the example wing section versus the thrust realized on a realistic benchmark airfoil.
- 6) Example 3D lifting body performance on an example platform of two a thin sheets: a lead aircraft towing a thin sheet platform.

**Basic Cambered Wing Section Performance** – A simple base case camber consisting of an arc of constant radius and thin enough to make the shapes of leading and trailing edges negligible was evaluated at several cambers and wing section pitches. Figure 2 summarizes key performance metrics of  $L/D$  efficiency and lift coefficient.

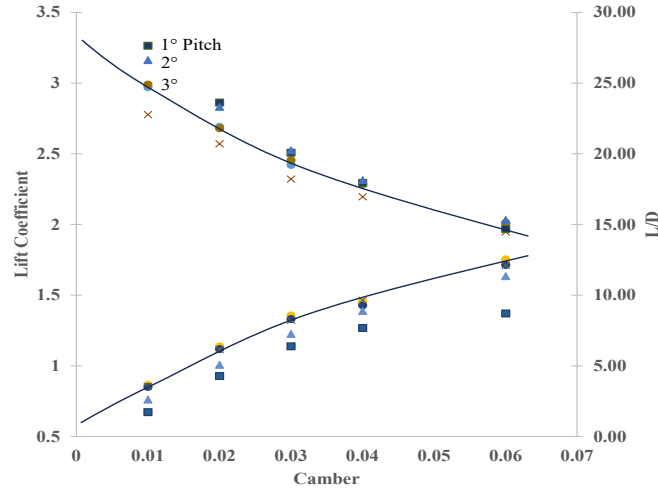


**Figure 2.** Impact of camber on lift coefficients, lower line is the lift coefficient based on 2D CFD.

While the highest  $L/D$  efficiencies are at low cambers, the lift coefficients, even for ideal wing sections, are too low to be useful. Higher cambers constantly generate aerodynamic lift along the chord, compensating for vertical dissipation of lift and generating higher  $L/D$  efficiency [30].

Wing section  $L/D$  efficiencies in excess of 40 can be attained by optimizing leading and trailing edges and by optimizing the camber. However, application of the wing sections as high aspect ratio wings is not practical since the wing sections lack the structural strength to transfer lift forces across the wing's span. Simple application in low aspect ratio designs, results in the spanwise dissipation of lift forces and low  $L/D$  efficiency. Applications in hang gliders and kites are able to function at these lower  $L/D$  efficiencies; however, the  $L/D$  efficiencies tend to be too low for commercial applications.

Two applications that have commercial potential are: a) propulsion-enhanced  $L/D$  efficiencies and b) use of thin cambered airfoils in ground effect [6]. For applications where air-based propulsion is required, synergies with the required propulsion can increase the effective  $L/D$  efficiency; which is particularly advantageous with bifacial sheets. For applications in ground effect, optimal configurations are able to block most of the downward and spanwise dissipation of lift pressures from the lower surface, which can be particularly advantageous as ultralight extensions of more-robust lifting body configurations.

**Basic Distributed Propulsion Studies** – Air-based propulsion generates lower pressures at propulsor intakes and higher pressures at propulsor discharges. Preliminary studies evaluated the use of a propulsor on a thin flat plate airfoil at leading-edge, mid-chord, and trailing edge locations on both upper and lower surfaces. The purpose was to identify instances of constructive versus destructive interference of propulsors with lifting body surfaces. Figure 3 summarizes the pressure profiles and Table 3 summarizes the  $L/D$  efficiencies.

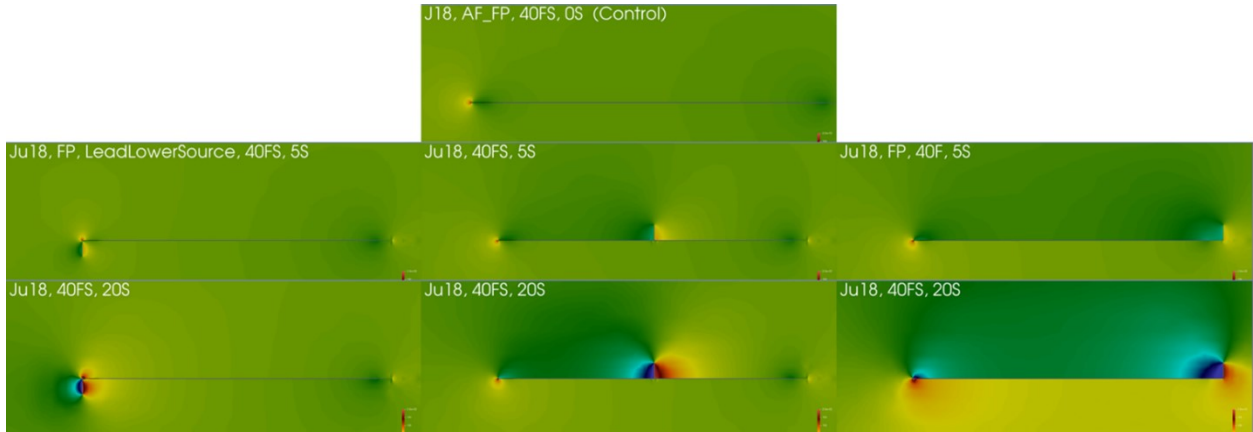


**Figure 3.** Use of Propulsors at three locations with two power settings each on a flat plate airfoil at  $0^\circ \alpha_P$ . From left to right, the propulsor is located at the lower-surface leading edge, upper-surface mid-chord, and upper-surface trailing edge.

Table 3 summarizes the  $L/D$  efficiencies corresponding to Figure 3. At an  $L/D$  efficiency of 21.8, the upper-surface trailing-edge propulsor is the only configuration having significant positive constructive interference.

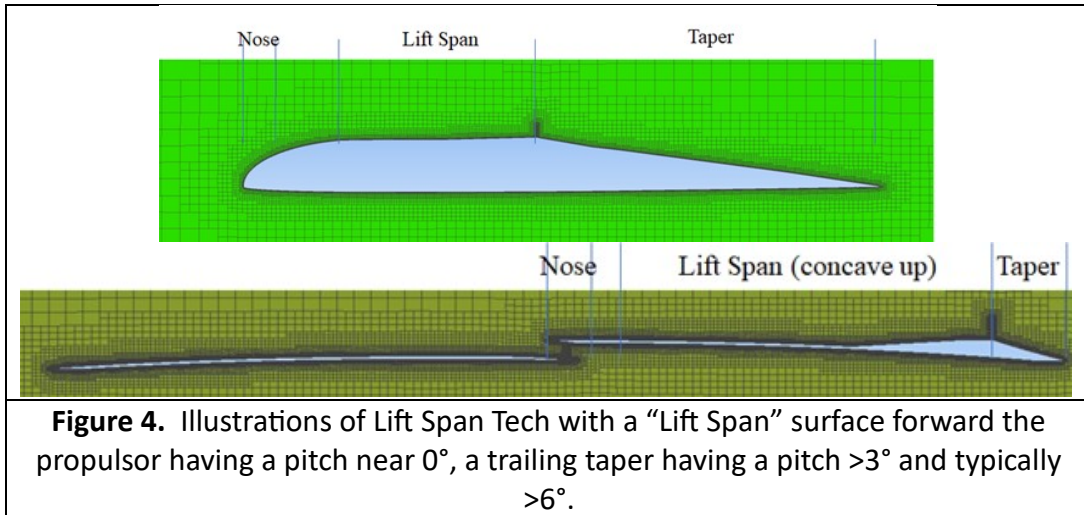
**Table 3. Performance of propulsion propulsors on flat plate airfoil.**

Propulsor and Pitch			Upper Propulsor			Lower Propulsor		
Lead/ Trail	Deg	Power	Cl	Cd	L/D	Cl	Cd	L/D
0	0	0	0.00	0.00	0			
Lead	0	20	-0.0054	0.0112	-0.5	0.0054	0.0112	0.5
Mid	0	20	0.0076	0.0089	0.8	-0.0076	0.0089	-0.8
Trail	0	20	0.1740	0.0080	<b>21.8</b>	-0.1740	0.0080	-21.8
0	1	0	0.0891	0.0090	9.9			
Trail	1	20	0.2840	0.0121	<b>23.5</b>	0.0894	0.0133	6.7
0	3	0	0.2830	0.0215	13.2			
Trail	3	20	0.4910	0.0324	<b>15.2</b>	0.2960	0.0261	11.3
Middle Propulsor								
Afore	3	80	0.3080	0.0290	10.6			
Afore	3	200	0.3370	0.0413	8.2			

Problems arise for an upper-surface trailing-edge propulsor location when the pitch of the surface prior to the propulsor exceeds  $3^\circ$ . The local surface  $L/D$  efficiency of an upper surface is provided by the following principle of basic physics referred to as Principle 4:

**Principle 4.** The  $L/D$  of a section of an airplane surface is approximately equal to  $57^\circ$  divided by the pitch of the surface in degrees for lower surfaces and  $-57^\circ$  divided by the pitch for upper surfaces. The pitch angle is relative to horizontal with the nose up as positive.

At 3° pitch an  $L/D$  of 19 is generated by lift pressures. Selecting a threshold  $L/D$  efficiency is consistent with targeting a lifting-body  $L/D$  efficiency greater than 19. This constraint is problematic for NACA-type airfoils which are both thicker and have upper-surface trailing-edge surface area pitches considerably greater than 3° in cruising configurations. Figure 4 illustrates Lift Span Tech, which is a technology designed to overcome this problem inherent in the placement of a propulsor at the upper-surface trailing edge.



**Basic Studies on Lift Span Technology** – Lift Span Tech consists of a near-horizontal surface in front of a trailing-section upper-surface propulsor and a Trailing Taper aft the propulsor. Figure 5 and Table 4 summarize performances of two Lift Span Configurations.

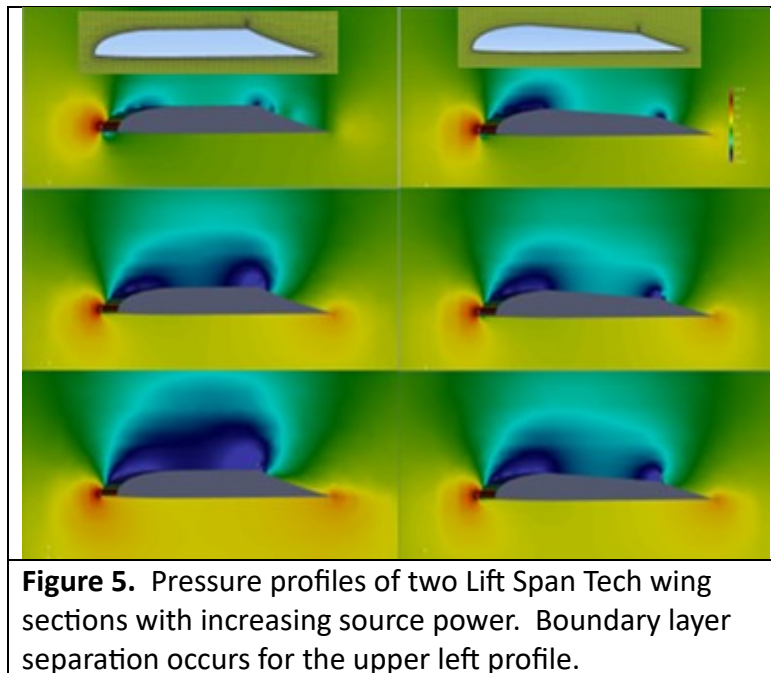


**Table 4.** Summary of  $L/D$  efficiencies and conditions for the two Lift Span Tech configurations of Figure 5.

FS (m/s)	S ( $m^4/s^2$ )	-1° Lift Span			4° Lift Span		
		$C_l$	$C_d$	L/D	$C_l$	$C_d$	L/D
40	0	0.251	0.0338	7.4	0.339	0.0219	15.5
40	20	0.527	0.0157	33.5	0.477	0.0186	25.6
40	40	0.607	0.0092	65.8	0.548	0.0163	33.6

Three significant findings as a result of Figure 5 include:

1. Lift Span Tech is effective in overcoming the issue of induced drag created by trailing-section upper-surface propulsors.
2. Boundary layer separation occurs on configurations with steeper Trailing Taper configurations and is overcome with a properly configured and operated trailing-section upper-surface propulsor.
3. Optimal applications of Lift Span Tech use surfaces where the pitch of the Lift Span decreases with increasing power setting.

More-detailed studies of Lift Span Tech are available elsewhere [25].

Figure 6 illustrates the use of Lift Span Tech on an aircraft platform comprised primarily of single-sheet planform areas.

**Mid-Chord Cross-Over Propulsor** - Further studies elucidate impacts of camber and use of both mid-chord and trailing-edge Propulsors. Figure 6 provides representative pressure profiles for a mid-section Propulsor with trailing Propulsors. The airfoil sections have a portion of the mid-chord propulsor between the leading airfoil section and the trailing airfoil section. The Figure 6 airfoils reveal:

- A convex upward camber can improve the performance of the mid-chord propulsor since discharged air diverges slightly from the surface to reduce the magnitude of the higher-pressure region aft of the Propulsor.
- As stronger trailing Propulsors are used in addition to the mid-section Propulsor, the trailing Propulsor is sufficient to create the leading-edge curl; the advantages of the mid-chord propulsor diminish with the higher power for the trailing-edge Propulsor.

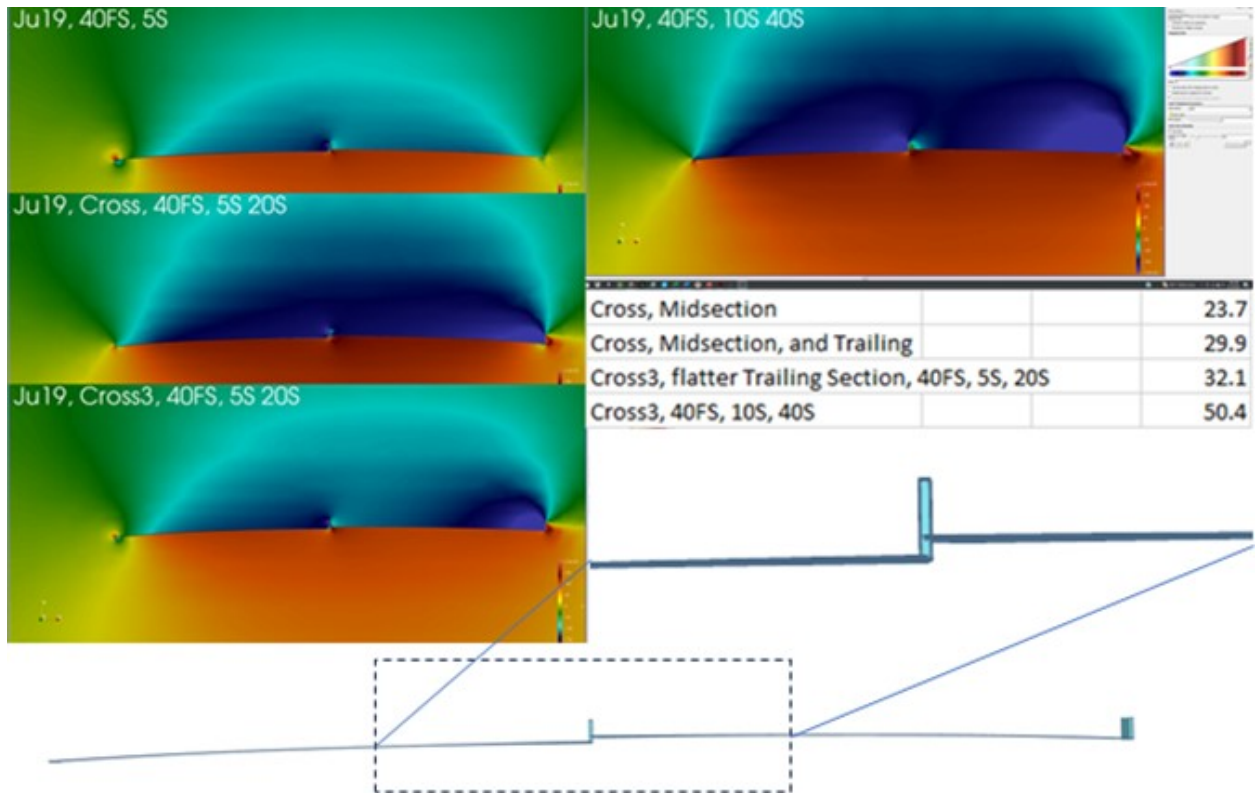


**Figure 6. Illustration of preferred mid-chord propulsor with representative pressure profiles and performance for wing sections. The Propulsor extends above the leading edge of the trailing airfoil subsection.  $L/D$  values are provided in the inset table.**

A mid-chord propulsor also impacts aspects of performance that can mitigate side losses; the investigation of side-edge loss mitigation is outside the scope of this paper.

Part of the discharge of the Figure 6 mid-chord propulsor flows under the leading edge of the trailing airfoil section. The thinner the trailing/leading edges interfacing with a mid-chord propulsor, the more effective the mid-chord propulsor performance is on improving  $L/D$  (per additional CFD results, not shown). A mid-chord crossover propulsor is primarily effective with thin-plate cambered airfoils. Ideally, the leading-edge of the trailing airfoil section is knife-sharp to minimize the higher-pressure air formation by the mid-section leading edge.

The leading airfoil sections of Figure 6 airfoils have an  $\alpha_A \approx -1^\circ$  to garner the advantages of induced thrust. The trailing airfoil sections have an  $\alpha_A \approx 1^\circ$ . Figure 7 provides separate pressure profiles for the isolated leading and trailing airfoils of Figure 6.

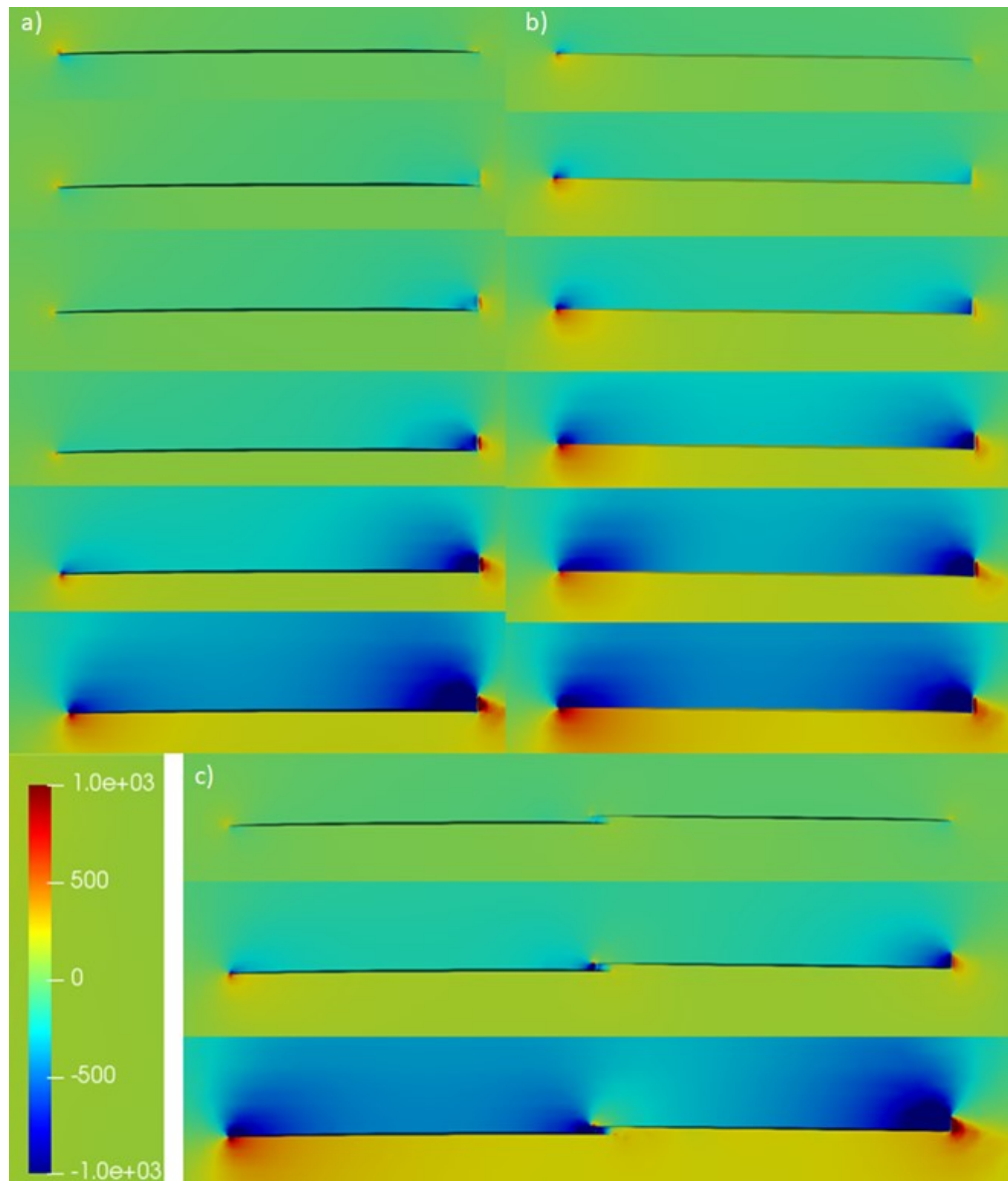


**Figure 7. Pressure profiles of an airfoil with mid-chord propulsor along with pressure profiles of the airfoil sections. No portion of the mid-chord propulsor extends above the leading edge of the trailing airfoil.**

When evaluated independently, the leading-airfoil subsection has a negative lift at lower Propulsor settings. This is due to free stream air impacting the upper surface and diverging from the lower surface. A trailing-edge Propulsor on the leading-airfoil subsection is able to overwhelm the impact of free stream velocities because the Propulsor intake forms lower pressures on an upper surface at  $\alpha_p \approx 0^\circ$ ; the lower-pressure air directly creates a strong lift force and indirectly extends forward to form a favorable leading-edge curl. The resulting  $L/D$  of the isolated leading section would continue to increase with increasing Propulsor setting; however, the induced thrust is a force through a distance, which translates to a thermodynamic constraint of a reduced gain-loss ratio of reduced drag versus reduced Propulsor thrust (i.e., increased

Propulsor *Loss* occurs at higher settings).

The independently-evaluated trailing airfoil (Figure 7b) has reasonable *L/D* based only on interaction with free stream velocities. Zero induced thrust is formed due to an  $\alpha_P > 0^\circ$ . The benefits of constantly increasing Propulsor power are limited by  $\alpha_P > 1^\circ$  at the Propulsor intake.

Figure 7 provides pressure profiles of the Figure 5c sequence at additional Propulsor settings. Tables 5 and 6 summarize the *L/D* of this airfoil sequence. At trailing Propulsor settings of 0, 20, and 80 with 25% mid-chord power, the airfoil towed planform configuration has *L/D* of 4.97, 22.5, and 35.2, while the Figure 8 airfoil configuration has *L/D* of 8.5, 12.0, 31.7, and 36.7. This identifies that while working in concert, both Propulsor terms are beneficial to the performance, but overall trends remain dominated by trailing-edge Propulsors in 2D simulations.

**Table 5. Parameters for Figure 7 airfoils.**

Mid-Chord propulsor Setting ( $m^4/s^2$ )	Trailing Propulsor Setting ( $m^4/s^2$ )	L/D
<b>Lead Airfoil, Figure 7a</b>		
N/A	1	-1.49
N/A	5	5.36
N/A	10	11.0
N/A	20	20.0
N/A	40	33.3
N/A	80	49.4
<b>Trailing Airfoil, Figure 7b</b>		
N/A	1	10.5
N/A	5	19.1
N/A	10	25.1
N/A	20	33.2
N/A	40	39.6
N/A	80	41.5
<b>Airfoil Sequence, Figure 7c</b>		
0	0	4.97
5	20	22.5
20	80	35.3

**Table 6. Parameters for Figure 8 airfoils.**

Mid-Chord propulsor Setting ( $m^4/s^2$ )	Trailing Propulsor Setting ( $m^4/s^2$ )	$C_l$	$C_d$	L/D
0	0	0.0735	0.0086	8.5;
20	0	0.0601	0.0050	12.0;
0	20	0.2914	0.0918	31.7
15	20	0.2722	0.0741	36.7.

The pressure profiles of Figure 8 illustrate how the mid-chord propulsor improves performance. As compared to a control with Propulsor terms off, a mid-chord propulsor power setting of 20 increases the  $L/D$  from 8.5 to 12.0 (Figs. 6a and 6b) with no trailing Propulsor. The primary mechanism for increasing  $L/D$  is the decrease of drag caused by transferring leading-edge higher-pressure air away from the front edges. A secondary mechanism for increasing  $L/D$  is generating lower pressures above the leading section and higher pressures below the trailing section through intake and discharge. Performance is dependent on the thickness and shape of the forward section of the trailing planform to reduce the higher-pressure region formed by the leading edge of the trailing section.

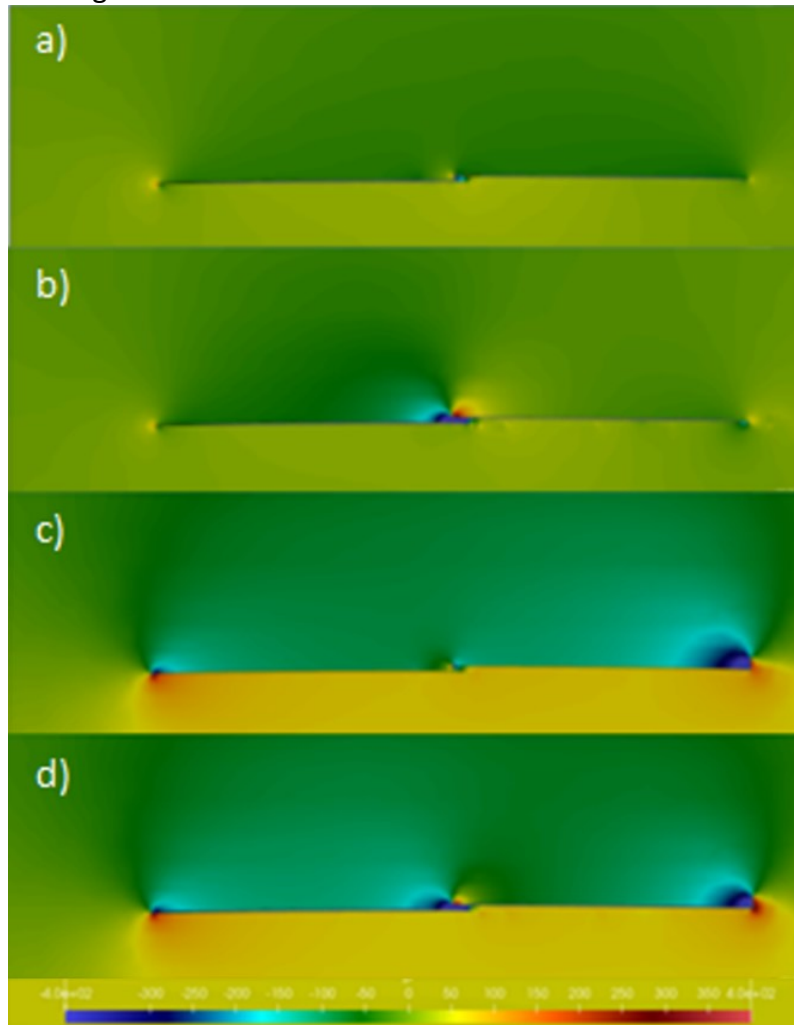


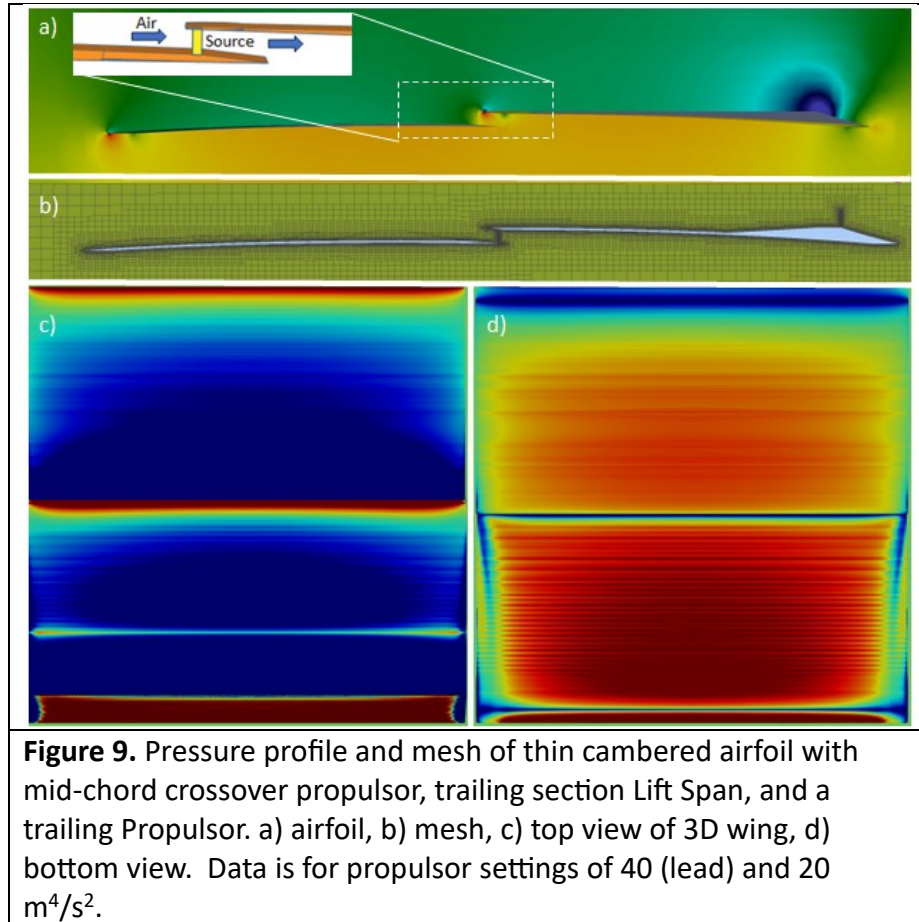
**Figure 8. Illustration of benefits of mid-chord propulsors. For the 0.01 c airfoil the data of mid-chord propulsor**

Use of a trailing Propulsor (20 power setting) without the mid-chord propulsor increases  $L/D$  from 8.5 to 31.7. The trailing-edge Propulsor improves the pressure profile throughout the airfoil with marked increases in  $L/D$ , provided the surface before the trailing Propulsor intake has  $\alpha_P < 2^\circ$ . The trailing-edge Propulsor decreases the magnitude of the higher-pressure region created by the mid-chord propulsor (Figure 8b versus Figure 8d).

The primary potential advantages of a mid-term Propulsor are related to mitigating the impact

of side-edge losses by a) mid-chord propulsors replenishing lift forces and b) creating air flow patterns that beneficially change the vectors of side-edge air flows. Studies of these potential advantages cannot be evaluated in the 2D CFD simulations of this paper.

**Digital Prototype Simulation** – Simulations results for a 3D prototype based on the accumulation of information from the wing sections is provided by Figure 9 and Table 7. The results are not optimized, but indicate that overall  $L/D$  efficiencies in excess of 20 are attainable for towed platform sequences.



The presence of induced drag, rather than induced thrust, at the leading edge indicates that the Figure 9 prototype is not operating at optimal conditions. Typically, a correction of this issue results in at least a 20% increase in  $L/D$  [30].

**Table 7.** Summary of  $L/D$  efficiencies of Figure 9 prototype.

Primary Propulsor	Mid Propulsor	$L/D$	$L/D$ front	$L/D$ back
20	5	<b>15.1</b>	11.8	17.4
40	5	<b>21.9</b>	13.0	30.0

40	10	<b>23.1</b>	14.0	40.5
40	20	<b>26.2</b>	14.5	-108.2

The trailing lifting body had the higher  $L/D$  efficiency, which can be attributed to the Lift Span Tech configuration of the trailing lifting body.

**Optimal Trailing Section Lift Span Tech Configurations** – Higher lift and higher  $L/D$  efficiency correlate with the formation of a robust trailing-edge stagnation point which expands along the lower surface and plays a role in neutralizing induced drag of aft surfaces. Figure 10 compares two spoiler geometries designed to enhance the trailing edge stagnation point for use with Lift Span Tech.

A trailing wing section, including spoilers, will tend to experience destructive interference from a leading wing section's pressures. The three-surfaced spoiler is designed to generate higher pressures on all surfaces; this can neutralize formation of negative lift and induced drag.

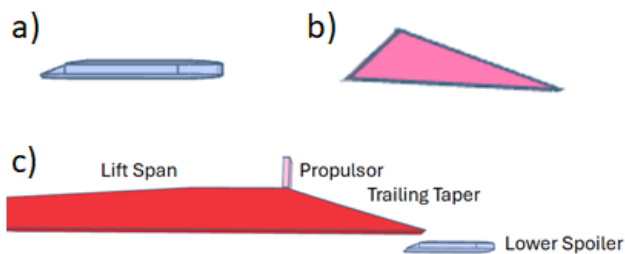


**Figure 10.** Illustration of spoilers evaluated at trailing edge stagnation point, where: a) horizontal plate with front taper, b) three-surfaced spoiler, and c) illustration of spoiler in relation to Lift Span Tech.

The assumption that placement of a stag-spoiler in the stagnation point unable to have negative effects since it is in stagnant air is erroneous; Care must be used to apply a spoiler appropriately. A stagnation point/region has constant air flow with higher pressures forming at a leading region, higher pressures dissipating at a trailing region, and from leading to trailing regions. Stagnation points/regions are not stagnant air. They are steady-state formation of higher pressures due to velocity-velocity air impacts or air flow impacting with a surface. Figure 11 illustrates how a three faced spoiler can be configured to change position and pitch depending on purpose.

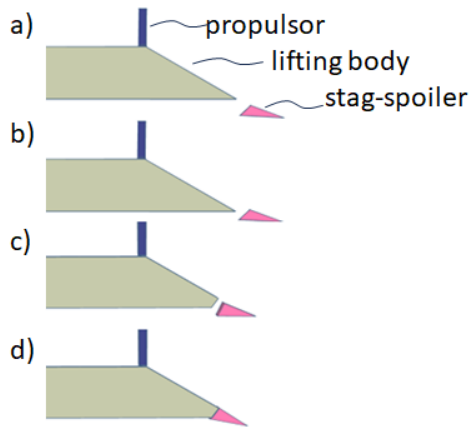


**Figure 11.** Illustration of three-faced spoiler to: a) impact with lower surface air flow, b) impact with both lower and trailing surface air flow, c) with lifting body conformed for contiguous flow connection, and d) in contiguous connection with lifting body as a flap.

Performances of the thin cambered airfoils with trailing edge spoilers are summarized by Table 8. The best performance was without a spoiler and with a flat trailing section lower surface at a propulsor setting of  $5 \text{ m}^4/\text{s}^2$  where unobstructed flows from the lower surfaces and the trailing taper impacted with the greater force to create higher stagnation point pressures.

**Table 8.** Comparison of performances of stagnation point spoilers.

Values do not account for pressures on spoilers.

	$S \text{ (m}^4/\text{s}^2)$	$L/D$	$C_{pD} / C_{vD}$
3-faced Spoiler	0	10.2	0.82
	2.5	13.8	0.93
	5	23.5	1.29
No Spoiler (Figure 13b)	0	10.6	0.65
	2.5	16.1	0.73
	5	25.6	1.33
Concave Control (Figure 13a)	0	9.7	1.26
	2.5	12.7	1.43
	5	15.4	1.74
Flat Spoiler	0	16.0	0.30
	2.5	20.6	0.23
	5	24.7	0.18

As illustrated by Figure 12, the three-faced spoiler is able to produce higher pressures on all surfaces. Absent forces on the spoilers, the wing section next to the flat spoiler had higher  $L/D$  efficiency than versus next to the three-faced spoiler; this comparison is misleading. The flat spoiler exhibits significant negative lift and induced drag in its position and the strong stagnation point increased the thin cambered airfoil's  $L/D$ . The primary mechanism for the flat spoiler toward increasing  $L/D$  efficiency was by reducing the pressure drag where the resultant higher pressures created an induced thrust on the thin cambered airfoil.

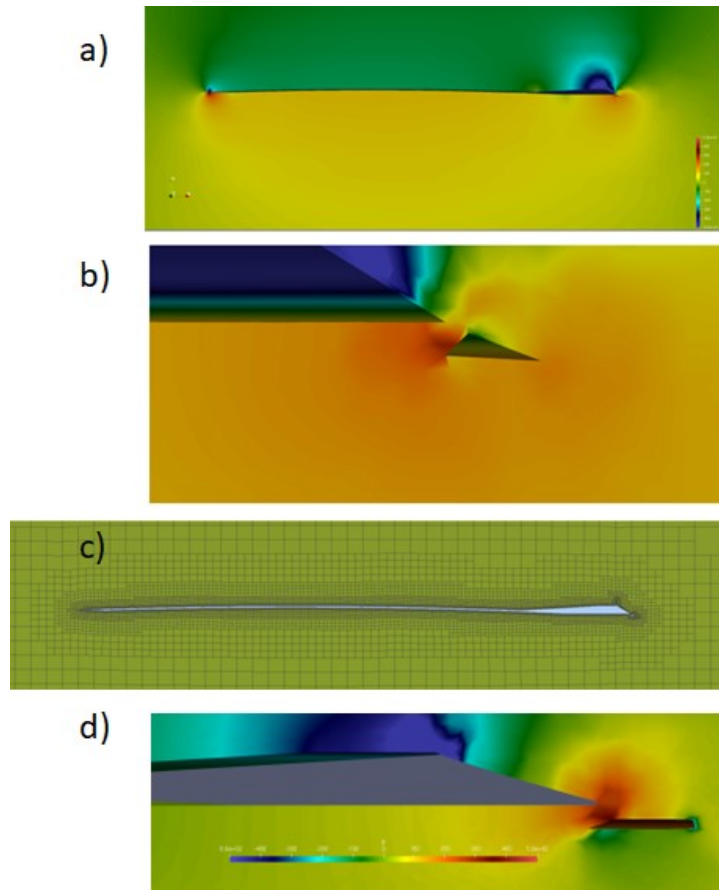


**Figure 12.** Illustration of three-faced spoiler wing sections: a) pressure profile with sheet wing section, b) close up of 3-faced spoiler pressure profile, c) CFD mesh, and d) pressure profile, and d) comparative image of flat plate spoiler.

Figure 13 compares the thin cambered airfoil with and without a flat horizontal lower surface on the trailing taper. The concave-down configuration has a higher pressure drag due to the greater frontal-projected area.



**Figure 13.** Comparison of control wing section (a) to wing section with trailing section of lower concave surface replaces with horizontally-flat surface(b).

## Discussion

### Overarching Trends

Table 9 compares the  $L/D$  for the flat plate airfoil of Figure 6 and the cambered airfoil of Figure 7. Thin flat plate airfoils are substantially lacking surfaces conducive to induce thrust. A trailing-section asymmetry creates lift at  $\alpha_A = 0^\circ$ , but the lift coefficient is very low at 0.047. As  $\alpha_A = 0^\circ$  increases, the  $L/D$  of a flat plate airfoil approaches a simple relation of  $L/D = \alpha_A^\circ / 57.3$ .

**Table 9.** Comparison of flat plate,  $L/D = \alpha_A^\circ / 57.3$ , and 0.03 camber 0.01 t/c airfoil with increasing camber at leading and trailing edges and trailing edge taper [30]

Pitch Angle ( $^\circ$ )	Flat Plate $C_L$	Flat Plate $L/D$	0.03 Camber $C_L$	0.03 Camber $L/D$	$\alpha_A^\circ / 57.3$
0	0.047	16.8	0.652	67.5	0
1	0.15	24.5	0.752	66	57.3
3	0.36	17	0.919	41	19.1
6	0.73	9.1	1.09	18.7	9.55

The induced thrust created by leading-section lower pressures is a critical feature enabling contemporary airfoils to achieve high  $L/D$ . Similar to contemporary airfoils, well-designed cambered airfoils are able to capitalize on induced thrust to increase  $L/D$ . Lift coefficients increase with increasing camber and  $\alpha_A^\circ$  for higher  $L/D$  thin-plate cambered airfoils.

Continuously curving surfaces, like a cambered surface, prevent the formation of straight-parallel flow and improves  $L/D$  by creating continuously diverging flow on upper surfaces and converging flow on lower surfaces. As the camber of a thin plate airfoil approaches 0 (i.e., a 0.01 c), the upper limit of performance is limited by  $L/D = \alpha_A^\circ / 57.3$  as with flat plates.

Figure 3 and Table 3 illustrate how a trailing-edge upper-surface propulsor can create lift and generally improve the lift-generating pressure profile throughout the airfoil. A trailing edge taper can achieve the same result where a sudden change in upper surface pitch generates lower pressures per Table 9. Numeric methods can be used to estimate the “effective thrust” provided by propulsors designed to influence pressure profiles on an airfoil [31].

As illustrated by Figure 14, the partial derivative of the “effective thrust” on an airfoil versus propulsor power setting has maximum magnitudes as the power setting approaches zero. At lower power, the Propulsor both reduces drag (i.e. converts drag to induced thrust) and increases lift. The Propulsor creates lower pressures on surfaces afore the Propulsor intake, a surface area referred to as the “Lift Span”. Lower pressure on a Lift Span with surface of  $\alpha_P < 0^\circ$  simultaneously increases the numerator and decreases the denominator of  $L/D$  for significant increases. As Propulsor power increases, the airfoil’s drag plateaus and the values of the partial derivative approach zero as shown in Figure 14.

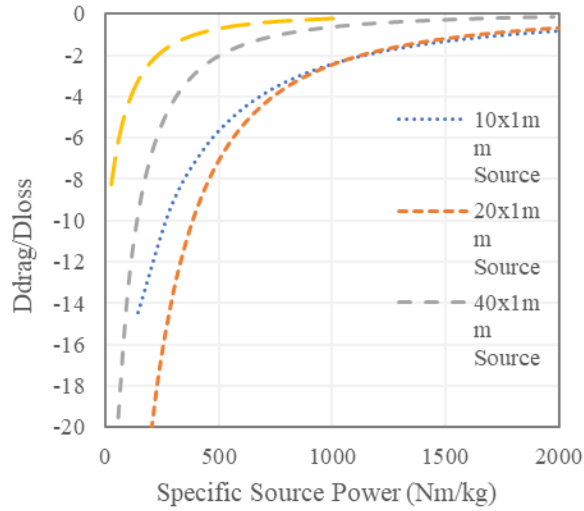


**Figure 14. Differential Gain-to-Loss ratio of power settings of trailing-edge Propulsor of differing heights on a symmetric 0.01 camber airfoil at 0° pitch elliptic shape.**

Figure 15 reports the numerical integrals of the partial derivatives as reported by Figure 14. Typically, as the power of a properly configured trailing-edge Propulsor increases, increasing amounts of power and energy are saved. The extent to which the power of the Propulsor increases depends on the power needs of the entire airframe and the fraction of the total power provided by the respective trailing-edge Propulsor. The Propulsor's lost thrust is from choking of the intake due to decreasing pressures before the Propulsor. The loss in Propulsor thrust can be leveraged in excess of 10X efficiency through use to eliminate drag beyond expected useful values.

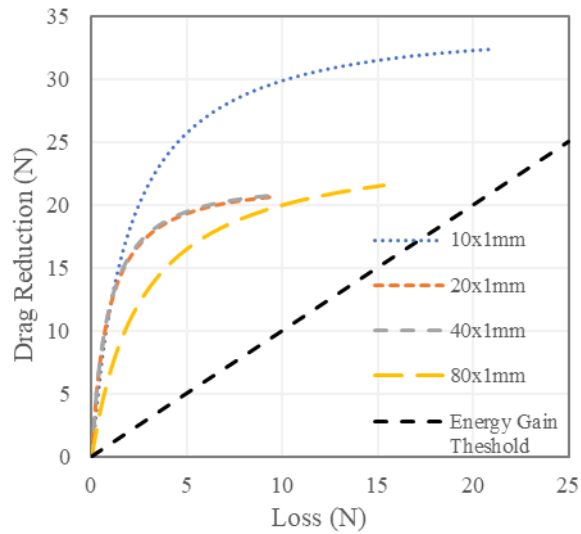


**Figure 15. Power savings due to reduced drag as Propulsor power increases vs loss of the Propulsor term. These results are the negative of the integral of Figure 14 results.**

Further discussions of this topic are provided by supplemental papers [30, 31]. Similar to the

manner in which minor changes in an airfoil can dramatically change  $L/D$  efficiencies, such as the addition of a trailing taper to a flat plate or an increase in a trailing taper that induces boundary layer separation, relatively small perturbations by strategically-place propulsors can cause significant changes in performance. As identified by Figure 14, when this occurs the initial propulsor has high [gain]:[loss] ratios which decrease as propulsor power is increased.

**Mid-Chord propulsor versus Trailing-Edge Propulsor** - Figure 16 summarizes the separate  $L/D$  of the leading-airfoil section and the trailing-airfoil section with mid-chord and trailing-edge Propulsors for the Figure 8 sequence where the mid-chord propulsor is at 25% the power setting of the trailing edge Propulsor. The constantly increasing induced thrust of the leading section results in constantly increasing  $L/D$ . The  $L/D$  of the trailing section plateaus at a power setting of about 20, a value near  $57^\circ / 3^\circ$ . This can be attributed to a higher pressure region on the upper surface behind the mid-chord propulsor which increases while other areas of the surface have increasing lift pressures.

Figure 17 illustrates how a mid-chord cross-over propulsor markedly increases lift coefficients. The data is definitive that cross-over propulsor increases lift forces. However, data on improving  $L/D$  efficiency with a cross-over propulsor is less definitive, especially in 3D performance where surfaces experiencing increased drag are close to the cross-over propulsor while much of the surface that experiences increased lift is further from the cross-over source.

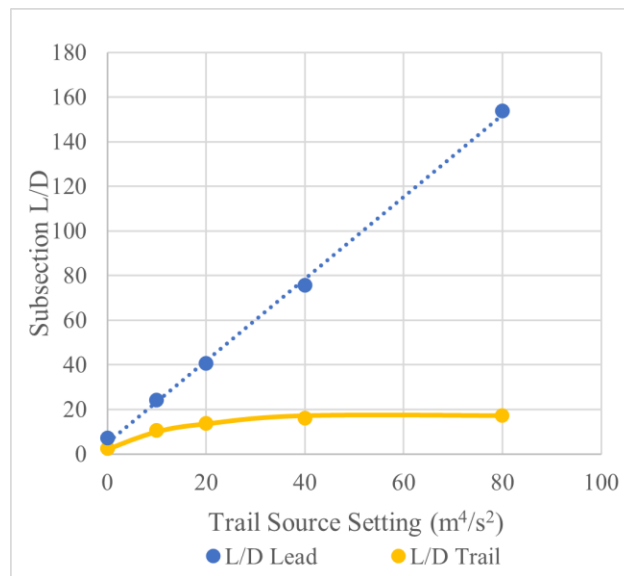


**Figure 16.  $L/D$  values for the leading-airfoil sections and trailing airfoil sections of Figure 8 which for sequential thin cambered airfoils with a crossover-propulsor transition.**

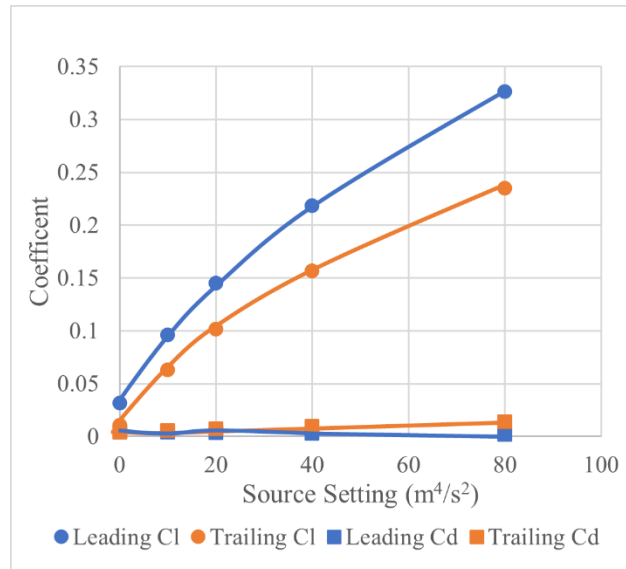


**Figure 17. Lift and drag coefficients of leading-airfoil sections and trailing airfoil sections of Figure 8.**

**Stagnation Point Spoiler** – While the comparison of thin cambered airfoil performance with and without stagnation point spoilers were not optimized to create the highest  $L/D$  efficiency, the following conclusions can be made:

- A three-faced spoiler can be configured to produce low spoiler drag and lift via higher pressures on all faces.
- A horizontal lower trailing-section surface below a Lift Span Tech section creates a stronger stagnation point and can lead to improved  $L/D$  efficiency.
- Distributed propulsion is a powerful degree of freedom to improve  $L/D$  efficiency of thin cambered airfoils.

**Weight and Sustainable Flight** – Due to the light weight of bifacial sheets, e.g. 0.076 kg/m<sup>2</sup>, bifacial sheets are able to produce much more power and lift than needed to sustain their own flight. As a result, good platform design dictates that lift be transferred from the sheets to compartments or that weight is distributed evenly throughout the bifacial sheet. Spars similar to the quills of a feather could transfer lift from the bifacial sheets to compartments, and the spars may act as battery storage configured within structural spars.  $L/D$  efficiencies of 10 to 20, as identified in lifting body prototypes of this paper, are more than adequate to make applications open-ended with capabilities beyond contemporary alternatives.

In addition to towed-platform airframes, bifacial sheets as trailing-extensions of highly-efficient wing-fuselage embodiments can extend the capabilities of electric aircraft.

**Implications of Power Ratios > 100** – The combination of Power Ratios > 100 along with identified  $L/D$  of the towed platforms of >15 indicate that towed platforms are able to systematically produce more power than consumed to sustain their flight. Previous figures summarized performance for thin wing sections suitable for drones. Figure 18 and Table 10 summarize performance of a thin cambered wing section following a thicker airfoil consistent with contemporary wings and lifting-body fuselages as used for passenger service.

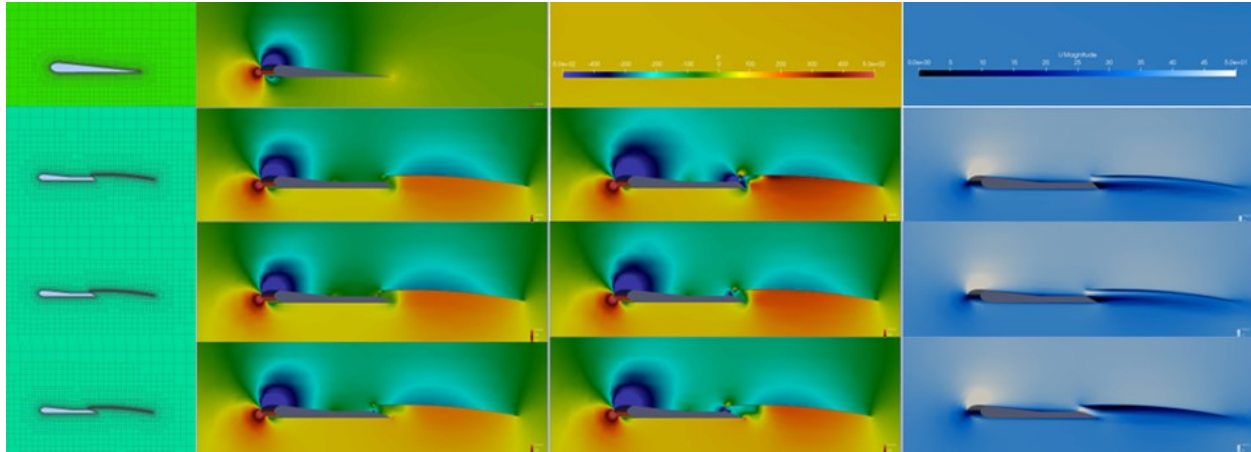


**Figure 18.** Pressure and velocity profiles of thin cambered wing section trailing a lead airfoil. Rows are for the same airfoil. Left-most are representative meshes. Pressure profiles are for 0 (left) and 10 (right) propulsor settings in  $\text{m}^4/\text{s}^2$ , and velocity profiles (rightmost). Free stream velocity is 20 m/s.

**Table 10.** Performance of Figure 18 wing sections.

	$S(\text{m}^4/\text{s}^2)$	Taper	L/D	$C_{dP}/C_{dV}$
Benchmark	0		12.0	2.6
Lead Airfoil	0	45°	21.7	2.5
	1	45°	21.9	2.5
	10	45°	21.8	3.0
	0	30°	19.9	2.7
	10	30°	21.2	3.3
	0	20°	23.2	2.8
	1	20°	23.1	2.9
	10	20°	21.0	3.7
Trailing	1	20°	10.2	8.8
	10	20°	7.3	9.5

Figure 18 illustrates the formation of good pressure profiles on both the lead airfoil and the trailing thin cambered airfoil. For contemporary airfoils, a good pressure profile typically consists of high-magnitude lower-pressure regions near the upper-surface apex. This feature enables good  $L/D$  efficiency over a range of pitch angles. For a trailing platform, the pressure distribution is more-evenly distributed along the airfoil.

The  $L/D$  efficiency of the lead airfoil ranged from 19.9 to 23.2 while the trailing thin cambered airfoil  $L/D$  efficiency ranged from 7.3 to 10.2. The lower  $L/D$  efficiency of the trailing airfoil was due to the lift pressures acting on high pitch-angle surfaces which can be corrected with Lift Span Tech such as that of Figure 13b. The higher performance of the lead airfoil with a

20° taper can be attributed to the formation of a trailing edge stagnation point which increases pressures on the airfoil's lower surface.

The formation of the trailing-edge stagnation point is due to the velocity from the propulsor hugging the trailing tapers upper surface rather than remaining adjacent to the trailing airfoil's lower surface. In the gap between the leading and trailing airfoils, all combinations have both higher and lower velocity streams; the optimal configuration would produce a constant velocity similar to free stream velocity. This adjustment would improve performance.

The Figure 18 data demonstrate the proof of concept for higher Power Ratio thin cambered airfoils a longitudinal extensions of more-contemporary wings. The following are possible with these bifacial sheets as longitudinal extensions of contemporary wings:

- Longitudinal transfer of lift even when not generating solar power and at sufficient  $L/D$  so as not to detract from efficiency.
- Ability to provide ultra-high-efficiency ground effect flight for takeoff, landing, and opportunity-based transit; this includes low-aspect-ratio designs that increase the versatility of takeoff and landing fields.
- Increased lift and enabling of lower-aspect ratio aircraft.
- Mitigation of boundary layer separation [31].

Additional results-directed optimization is warranted with optimal configurations and operation dependent on application.

## Conclusions

Aircraft platform areas consisting of single bifacial sheets provide advantages of higher power densities ( $W/m^2$ ); but conventional aircraft platforms using single-sheet platform construction, like hang gliders, have poor  $L/D$  efficiencies. Low-aspect-ratio aerial towed platform technology enables flexible designs that are more robust than ultralight high-aspect-ratio platforms. This enables the same platform to be used for 24/7 HAPS/HALE and day-mission aircraft. Using the same platform can bring economies of scale and increase versatility.

Towed platform technology and distributed propulsion technology provide additional degrees of freedom which can provide higher  $L/D$  efficiencies with increased capabilities for solar aircraft. Towed platform technology provides passive stability and a robustness founded in flexibility. Two distributed propulsion technologies are able to improve performance: a) Lift Span Tech is effective to increase lift and  $L/D$  efficiency and b) Cross-Over Propulsors are effective for increasing lift but their ability to increase  $L/D$  efficiency is less definitive. Cross-Over propulsors extend the effect of camber for additional sequential towed platforms.

For optimal performance, the propulsors are coordinated with lifting body surfaces around the propulsor and optimal surfaces which vary with propulsor power. Preliminary data identify that  $L/D$  efficiencies in excess of 20 are possible for towed platforms. The towed platforms can be used as trailing extensions on lead aircraft with higher  $L/D$  efficiencies.

Bifacial sheets can be used in both thin-lifting-body drone aircraft and as longitudinal augmentations of wings on larger fuselages. As wing augmentations, the sheets and distributed propulsion can collect power, increase lift, and prevent boundary layer separation; The proofs of

concept are presented with results-driven optimization being application-dependent.

## References

- [1] Deline, C., Palaez, S.A., Marion, B., Sekulic, B., Woodhouse, M., and Stein, J., "Bifacial PV System Performance: Separating Fact from Fiction," 2019 <https://www.nrel.gov/docs/fy19osti/74090.pdf> [cited Nov 27 2023].
- [2] Burgmann, S. Dannemann, J. & Schroder, W., "Time-resolved and volumetric PIV measurements of a transitional separation bubble on an SD7003 airfoil | SpringerLink," *Experiments in Fluids*, Vol. 44, 2007, pp. 609–622. <https://doi.org/10.1007/s00348-007-0421-0>
- [3] Michna, J., and Rogowski, K., "Numerical Study of the Effect of the Reynolds Number and the Turbulence Intensity on the Performance of the NACA 0018 Airfoil at the Low Reynolds Number Regime," *Processes*, Vol. 10, 2022, pp. 1004. 10.3390/pr10051004
- [4] McDonald, R.A., German, B.J., Takahashi, T., Bil, C., Anemaat, W., Chaput, A., Vos, R., and Harrison, N., "Future aircraft concepts and design methods," *The Aeronautical Journal*, Vol. 126, No. 1295, 2022, pp. 92–124. 10.1017/aer.2021.110
- [5] Sears, W.R., "Some Recent Developments in Airfoil Theory," *Journal of the Aeronautical Sciences*, Vol. 23, No. 5, 1956, pp. 490–499. 10.2514/8.3588
- [6] Suppes, G., and Suppes, A., "Ground Effect Flight Transit (GEFT) – Approaches to Design," Cambridge University Press, Cambridge Open Engage, 2024. <https://www.cambridge.org/engage/coe/article-details/66b2340b01103d79c5e7ab23>10.33774/coe-2024-2c87q

- [7] Winslow, J., Otsuka, H., Govindarajan, B., and Chopra, I., "Basic Understanding of Airfoil Characteristics at Low Reynolds Numbers (104–105)," *Journal of Aircraft*, Vol. 55, 2017, pp. 1–12. 10.2514/1.C034415
- [8] Traub, L., and Coffman, C., "Efficient Low-Reynolds-Number Airfoils," *Journal of Aircraft*, Vol. 56, 2019, pp. 1–17. 10.2514/1.C035515
- [9] Milgram, J.H., "Section data for thin, highly cambered airfoils in incompressible flow," 1971. <https://ntrs.nasa.gov/citations/19710020417>
- [10] Leifsson, L., Ko, A., Mason, W., Schetz, J., Haftka, R., and Grossman, B., "Multidisciplinary Design Optimization for a Blended Wing Body Transport Aircraft with Distributed Propulsion," 2011,
- [11] Klose, B., Spedding, G., and Jacobs, G., "Direct numerical simulation of cambered airfoil aerodynamics at  $Re = 20,000$ ," 2021, <https://doi.org/10.48550/arXiv.2108.04910>
- [12] Russo, O., and Arovitola A, de Rosa D, Pezzella G, Viviani A., "Computational Fluid Dynamics analyses of a wing with distributed electric propulsion," *Aerospace*, Vol. 10, No. 1, 2022, <https://doi.org/10.3390/aerospace10010064>
- [13] Serrano, J., Tiseira, A., García-Cuevas, L., and Varela, P., "Computational Study of the Propeller Position Effects in Wing-Mounted, Distributed Electric Propulsion with Boundary Layer Ingestion in a 25 kg Remotely Piloted Aircraft," *Drones*, Vol. 5, 2021, pp. 56. 10.3390/drones5030056
- [14] Felder, J., Brown, G., DaeKim, H., "Turboelectric Distributed Propulsion in a Hybrid Wing Body Aircraft," 12 September 2011,

[15] Kim, H.D., Perry, A.T., and Ansell, P.J., "A Review of Distributed Electric Propulsion Concepts for Air Vehicle Technology," *2018 AIAA/IEEE Electric Aircraft Technologies Symposium (EATS)*, 2018, pp. 1–21.

10.2514/6.2018-4998

[16] Gohardani, A., Doulgeris, G., and Singh, R., "Challenges of future aircraft propulsion: A review of distributed propulsion technology and its potential application for the all electric commercial aircraft,"

*Progress in Aerospace Sciences*, Vol. 47, 2011, pp. 369–391. 10.1016/j.paerosci.2010.09.001

[17] Finger, D., Braun, C., and Bil, C., "A review of configuration design for distributed propulsion transitioning VTOL aircraft," *2017 Asia-Pacific International Symposium on Aerospace Technology, Seoul, Korea*, 2017, pp. 1–15.

[18] Borer, N.K., Derlaga, J.M., Deere, K.A., "Comparison of Aero-Propulsive Performance Predictions for Distributed Propulsion Configurations," Grapevine, TX, January 9, 2017,

[19] Erhard, R., Clarke, M., and Alonso, J., "A Low-Cost Aero-Propulsive Analysis of Distributed Electric Propulsion Aircraft," January 11, 2021, 10.2514/6.2021-1200

[20] Achour, G., Sung, W., Pinon, O., "Development of a Conditional Generative Adversarial Network for Airfoil Shape Optimization," 2020-01-06, 10.2514/6.2020-2261

[21] Wu, R., Soutis, C., Zhong, S., and Filippone, A., "A morphing aerofoil with highly controllable aerodynamic performance," *The Aeronautical Journal*, Vol. 121, 2016, pp. 1–19. 10.1017/aer.2016.113

[22] Bulat, P., Chernyshov, P., Prodan, N., and Volkov, K., "Control of Aerodynamic Characteristics of Thick Airfoils at Low Reynolds Numbers Using Methods of Boundary Layer Control," *Fluids*, Vol. 9, No. 1, 2024, pp. 26. 10.3390/fluids9010026

[23] Ma, Y., Zhang, W., and Elham, A., "Multidisciplinary Design Optimization of Twin-Fuselage Aircraft with Boundary-Layer-Ingesting Distributed Propulsion," *Journal of Aircraft*, Vol. 59, 2022, 10.2514/1.C036559

[24] Suppes, G., and Suppes, A., "Critical Data and Thinking in Ground Effect Vehicle Design," Cambridge University Press, Cambridge Open Engage, 2024.

<https://www.cambridge.org/engage/https://doi.org/10.33774/coe-2024-76mzx>

[25] Suppes, A.B., and Suppes, G., "Thin Cambered Lifting Bodies in Ground Effect Flight," *Engrxix Engineering Archive Pre-Print*, No. 1, 2024, <https://doi.org/10.31224/4136>

[26] Sanches Bravo, A., "Project of an UAV of infinite autonomy," 2019.

[https://upcommons.upc.edu/bitstream/handle/2117/173460/Report\\_fitxer\\_de\\_consulta.pdf](https://upcommons.upc.edu/bitstream/handle/2117/173460/Report_fitxer_de_consulta.pdf)

[27] Moelyadi, M.A., and Zulkarnain, M.F., "HALE UAV ITB perpetual flight," *IOP Conference Series: Materials Science and Engineering*, Vol. 1109, No. 1, 2021, pp. 012028. 10.1088/1757-899X/1109/1/012028

[28] Smil, V., "Power Density Primer: Understanding the Spatial Dimension of the Unfolding Transition to Renewable Electricity Generation (Part IV – New Renewables Electricity Generation)," 2010,

<https://www.masterresource.org/smil-vaclav/smil-density-new-renewables-iv/>

[29] Lee, D., Nonomura, T., Oyama, A., and Fujii, K., "Comparison of Numerical Methods Evaluating Airfoil Aerodynamic Characteristics at Low Reynolds Number," *Journal of Aircraft*, Vol. 52, 2015, pp. 296–306. 10.2514/1.C032721

[30] Suppes, G., and Suppes, A., "Understanding Thin Cambered Airfoils and their Solar Aircraft Applications," *Research Square*, 2023, pp. 1–29. <https://doi.org/10.21203/rs.3.rs-4670250/v1>

[31] Suppes, A., and Suppes, G., "Thermodynamic Analysis of Distributed Propulsion," *Research Square*, 2023, pp. 1–26. 10.21203/rs.3.rs-4670270/v1